SPi | Journal Code: S I A | Article ID: 5 2 1 0 | Dispatch: 19.12.12 | CE: | No. of Pages: 10 | ME:

Research article

SURFACE and INTERFACE ANALYSIS

Received: 18 July 2012 Revised: 4 December 2012 Accepted: 4 December 2012 Published online in Wiley Online Library

(wileyonlinelibrary.com) DOI 10.1002/sia.5210

Surface modification of titanium by anodic oxidation in phosphoric acid at low potentials. Part 1. Structure, electronic properties and thickness of the anodic films

A. Gomez Sanchez,[a]* W. Schreiner,[b] G. Duffó[c,d] and S. Ceré[a]

ABSTRACT: Titanium surface characteristics determine the degree of success of permanent implants. The topography, morphology of the surface in micro and nano scales, the impurities present and other characteristics are a main concern, and therefore a multi-technique approach is required in order to evaluate modification process effects on the surface.

Surface modification of titanium in the nanometrical range was performed by means of anodisation in phosphoric with the aim of improving both the biocompatibility and the corrosion resistance in the biological media. Biocompatible characteristics of the modified titanium surface, as the presence of anatase in the oxide film and the incorporation of phosphate to the surface, were determined. Moreover, the electronic properties of the surface oxide presented a carrier number adequate for biomedical applications.

The increase in the film thickness from 3 to 42 nm was estimated from EIS results when anodising potentials from 0 to 30 V were applied, whereas a bi-layer structure of the protective oxides formed was determined. Copyright © 2012 John Wiley & Sons, Ltd.

Keywords: titanium; anodic oxides; biomaterials; surface modification; oxide film; structure

Introduction

The osseointegration capability of titanium and its alloys may be improved by surface modification in different length scales from a few microns to tens of nanometers.[1–4] With this aim, big efforts are being conducted in the development of better surface finishing of these materials, mainly devoted to the study of the effect of modification of the surface in the nano and microscale. The chemistry of the surface, topological features and also the electronic properties are believed to play important roles on the tissue response to materials implanted.[5]

Two design criteria are proposed to elaborate surface modification routes to improve osseointegration.

One is the coating of the metal surface with bioactive ceramics (hydroxyapatite or bioactive glasses). The osseointegration process is accelerated by the presence of Ca-P rich compounds, as was demonstrated by several authors.[6–8] Coating processes includes plasma spray,[9,10] magnetron sputtering,[11] cathodic electrodeposition,[12–14] electrophoresis [15–17] and biomimetic methods.[3,18–23]

In the other direction, the modification of the chemistry or the topography of the surfaces to induce them *in vivo* deposition of bioactive materials (apatite) or to promote cell adhesion or other specific responses of the tissue/material interactions are proposed. These methods include alkaline treatments,[24–28] peroxide immersion [29–31] acid immersion,[32,33] mechanical treatments to induce controlled roughness,[34,35] thermal treatments [36] and anodisation.[36–47]

Anodisation is presented as a non expensive one-step method to induce controlled chemical, topological and also electronic modifications on titanium surface. Acid and alkaline media and multiple processing parameters were explored. However, the relation of the anodisation process parameters with the surface characteristics of the oxide layer is still not fully developed, and therefore, an increasing number of articles are being published in this area.[48,49] Despite the numerous data available related to anodic film characteristics and *in vitro* and *in vivo* response, the strong influence of the anodisation parameters on the final surface condition gives a somehow contradictory picture of the modified surfaces performance, due to the spread of the results presented.

Additionally, the majority of the work is focused on anodisation at high potentials, near the breakdown of the oxides, with the aim of promoting high roughness in the micrometrical range. However, decrease in corrosion resistance,[42,50] poor bond strength to the metal substrate [51] and the presence of cracks [52,53] were found

* *Correspondence to: A. Gomez Sanchez, División corrosión - INTEMA, Universidad Nacional del Mar del Plata - CONICET, Juan B. Justo 4302, (7600) Mar del Plata, Argentina Email: aaguar@gmail.com*

a *División corrosión - INTEMA, Universidad Nacional del Mar del Plata - CONICET, Juan B. Justo 4302, 7600Mar del Plata, Argentina*

b *LSI – LANSEN, Departamento de Física UFPRCuritiba, Brasil*

c *Departamento de Materiales, Comisión Nacional de Energía Atómica – CONICET, Av. Gral. Paz 14991650, San Martín, Buenos Aires, Argentina*

d *Universidad Nacional de Gral. San Martín, Av. Gral. Paz 14991650, San Martín, Buenos Aires, Argentina*

UNCORRECTED PROOF

Copyright © 2012 John Wiley & Sons, Ltd.

in porous surface oxides growth in those conditions. Moreover, anodic films obtained at low potentials require lower cost equipment to perform the surface modification. In this context, a systematic study of the growth process, structure characterisation and electrochemical behaviour of anodic oxide films on titanium in a low potential range with respect to the breakdown potential in H_3PO_4 1 mol/l [45,51,54] is presented.

Experimental

Materials and surface modification treatment

Flat specimens of 20 × 15 × 0.127 mm of titanium grade 2 were used. A copper wire on one extreme of the sample was used as electrical contact, conveniently isolated from electrolyte.

The specimens were anodised in a two electrode cell, in 1mol/l H_3PO_4 solution at a constant potential difference between 3 and 30 V for 60 min. The samples conditioning and oxide growth details were previously reported.[55] Phosphoric acid was selected as the anodising electrolyte with the aim of promoting the incorporation of P to the oxide film.

Before and after each test, the samples were cleaned with acetone, dried in air and stored in a dryer.

Colors of anodic oxide films

The colors of anodic oxide films are the result of interference phenomenon of incident light on surface films. While anodic oxide colors are mainly related to the thickness of the films, there are several factors that influence the resulting color observed at each anodising condition. The main of them are: substrate roughness, non-uniform film thickness on the entire sample, the surface oxide stoichiometry, the presence of defects or impurities.[58] However, when starting conditions are maintained (i.e. substrate characteristics and electrolyte), the colors of oxide films can be used for a quick identification purpose of the resultant oxide thickness in association with the anodic forming voltage.[38]

With the aim of developing an accurate and systematic manner to facilitate the study of reproducibility, and to further relate with the film thickness, a computer program was developed by the Image Analysis Laboratory of the Electronic Department at the Faculty of Engineering of the National University of Mar del Plata. This software quantifies the contribution of the primary colors red, green and blue (RGB), according to the scale widely used in commercial programs for image analysis, on each pixel of high-resolution images of the samples. This program assigns a value between 0 and 255 for each primary colors contribution and finally determines the average for each color on the entire sample.

This method to characterise the coloration of anodic oxides was developed and successfully used to characterise zirconium anodic oxides,[55] and therefore the method was used to evaluate the colors obtained for each anodising condition on titanium.

Surface characterisation

The overall surface morphology of the specimens corresponding to all the anodising conditions was observed by scanning electron microcopy (SEM) (JEOL JSM-6460LV, Japan) at 15 kV. Surface elemental analysis was simultaneously determined by energy dispersive X-ray spectroscopy (EDS) (EDAX Genesis XM4 – Sys 60).

The surface topography was characterised by atomic force microscopy (AFM) using an AFM Agilent 550 in contact mode. Image analysis was performed with Gwyddeon free software. The roughness average (Ra) and root mean square roughness (RMS) parameters were determined on square regions with side lengths of 10 × 10 μm.

The crystalline phases corresponding to anodic oxides were determined by Raman spectroscopy using an Invia Reflex confocal Raman microprobe (Renishaw, UK). The Raman spectra were obtained using an argon laser of 514 nm using a 50× objective lens. No thermal effects were observed on the samples during the measurements.

Species present on the surfaces were identified by X-ray photoelectron spectroscopy (XPS) using a VG Microtech ESCA 3000 system. Survey scans and high-resolution detailed scans of the main spectral peaks detected in the survey spectra were recorded. All the values of the binding energy (BE) are referenced to a BE for C 1s of 284.5 eV.

Electrochemical studies

After anodisation, the electrodes were electrochemically studied in a conventional three-electrode cell using a saturated calomel electrode (Radiometer Analytical, France) as reference electrode and a platinum wire as counter electrode. The electrolyte used was 1 mol/l H_3PO_4. The electrode was stabilised for 40 min at open circuit potential before each measurement. Impedance measurements to obtain the corresponding Mott–Shottky plots [56] were performed at a fixed frequency of 1000 Hz. A 10 mV RMS perturbation signal was superimposed to a fixed potential, which was varied in a wide potential range using a Reference 600TM Potentiostat-Galvanostat-ZRA (Gamry Instruments, USA).

Electrochemical impedance spectroscopy (EIS) measurements were carried out using a PCI4 750/potentiostat/galvanostat/ZRATM (Gamry Instruments, USA). The amplitude of the perturbation signal was 10 mV RMS, and the impedance was measured between 10^{-2} and 10^{6} Hz. The impedance data was fitted to equivalent circuit models with Zplot for Windows software.[57]

Results and discussion

Surface characterisation of the anodic oxides

Color

Colors of the surface films obtained at each anodising potential on titanium, along with the RGB values determined and a digital image colored according to the values obtained are shown in Table 1. It was verified a good reproducibility of the RGB values attained for different samples anodised at the same potential, and for different images taken for a given sample..

It is known that the colors of surface oxide films on valve metals can be related to films thickness.[55] However, other characteristics as roughness, stoichiometry, homogeneity and defects influence the color of thin oxide films,[58] and they are the origin of discrepancies in anodic films on titanium obtained in similar conditions (and therefore, with similar thickness expected). Besides, a good correlation of colors obtained in this work is found when comparing colors reported for similar anodic growth conditions.[38,54,59,60] These results allow the method described to be used to check the reproducibility of the anodising process pointing to a future industrial process to typify the surface finish with an easy and cheap technique.

Surface morphology

SEM micrographs corresponding to titanium as-received and anodised at 30 V are presented in Fig. 1. No major evidence of

UNCORRECTED PROOF

Copyright © 2012 John Wiley & Sons, Ltd.

Table 1. Colors obtained after anodisation at different potentials. The corresponding red-green-blue (RGB) values digitally obtained are shown in the circle

Anodising condition	As received	3 V	6 V	12 V	18 V	24 V	30 V
	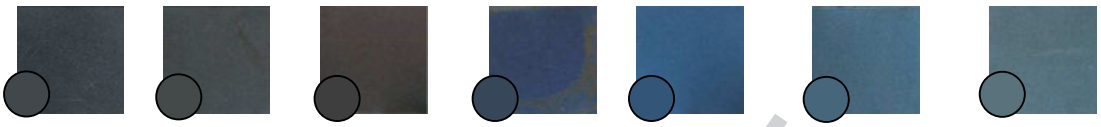						
Color	**Gold**	**Dark gold**	**Brown – violet**	**Blue – violet**	**Light blue**	**Light blue - green**	**Green**
R	65 ± 5	68 ± 1	63 ± 5	56 ± 1	51 ± 4	70 ± 2	90 ± 4
G	71 ± 5	73 ± 1	62 ± 3	70 ± 1	86 ± 5	102 ± 3	114 ± 2
B	75 ± 5	73 ± 1	62 ± 1	90 ± 4	120 ± 10	124 ± 1	124 ± 2

surface modification is observed on titanium surface. EDS spectrum presented in Fig. 2 shows the increase in oxygen proportion, evidenced by the increase of the corresponding peak, for anodised film with respect to the as-received titanium, together with the incorporation of P to the surface, further corroborated with XPS (See Figs. 6 and 7).

The morphology of the growing oxide was also observed with contact mode AFM. Besides the fact that the parallel band structure resulting from the lamination of the titanium sheets is observed as the main topology feature, globular structures covering the titanium surface were detected on anodised samples (Fig. 3). From AFM image analysis, the roughness parameters Ra and RMS were calculated. Both parameters remain almost constant (60–70 nm over a scaling surface of 10×10 μm) in all the anodised conditions. The low incidence of anodisation process on surface roughness is in agreement with previously reported results when the oxide films were growth at low potentials.[46,61]

Crystallographic phases corresponding to the anodic films on titanium

Titanium dioxide presents three main crystallographic phases: rutile, anatase and brookite.[64] Anodic growth conditions on titanium determine the degree of crystallinity and the crystallographic phases obtained.[65] Since then, a variety of results are reported. At low potentials, amorphous films were often found with XRD,[66] whereas in studies performed by transmission electronic microscopy, the presence of anatase and rutile phases was reported.[67–70] At intermediate potentials (with respect to the breakdown potential), various authors agree the presence

CORRECTED PROOF

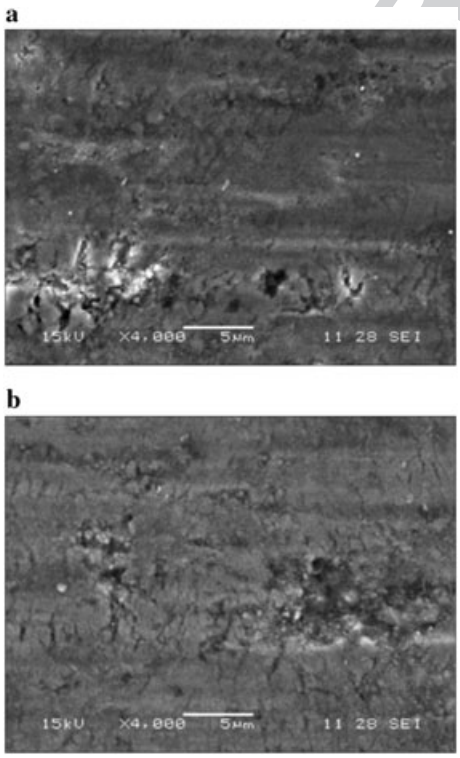

Figure 1. SEM micrographs of: **a**. As-received titanium. **b**. Titanium anodised at 30 V.

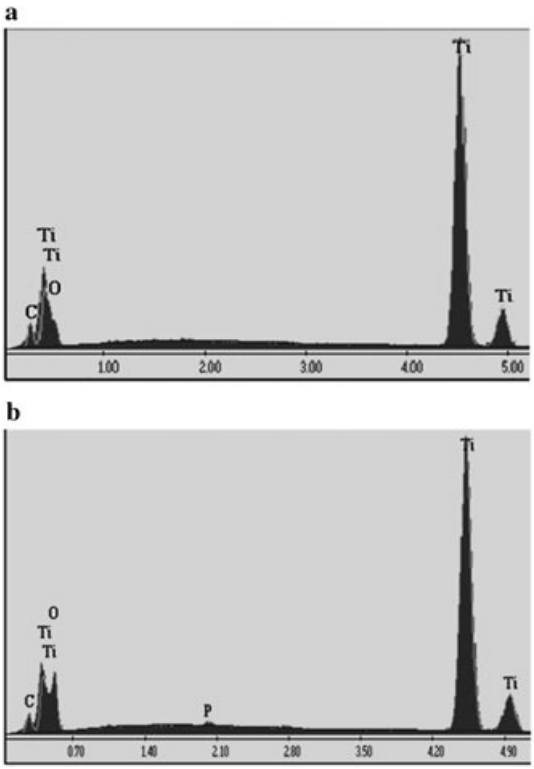

Figure 2. EDS spectra corresponding to titanium **a**. As-received **b**. Anodised at 30 V.

Copyright © 2012 John Wiley & Sons, Ltd.

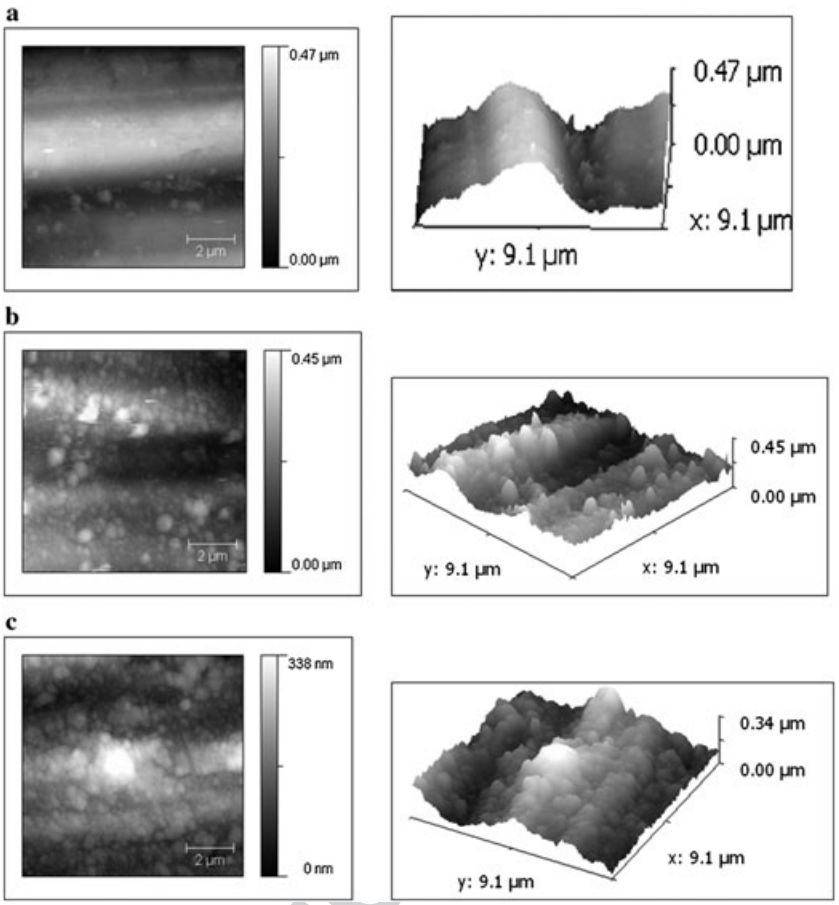

Figure 3. Contact mode AFM images of titanium **a**. As-received. **b**. Anodised at 18 V. **c**. Anodised at 30 V.

of a limited degree of crystallinity and a mixture of rutile and anatase.[71,72] In anodic films obtained at potentials higher than 100 V, where the film thickness is thicker than 200–300 nm, the correlation between the growing conditions and the degree of crystallinity and crystallographic phases presented have been determined with high detail with XRD, and a high influence of the anodisation parameters with the crystallographic structure was found.[39,47]

Although XRD is a powerful and versatile tool to characterise crystallographic phases of thin films, some authors stated that the technique fails when applying on anodic films on titanium due to the small thickness and partial crystallinity of oxide films obtained in some electrolytes, even at potentials near the breakdown potential.[72,73] In this work, the determination of crystalline phases of TiO_2 was not possible with XRD, even at low angles. Crystalline phases were determined by Raman spectroscopy in as-received titanium (Fig. 4) and in titanium anodised at 30 V (Fig. 5). The determination of various Raman spectra on different positions through a line made on an optical micrograph was performed with the aim of studying the growth morphology of the oxide films. Despite that the peaks detected with Raman spectroscopy were broad and with low intensity, evidencing the low crystallinity of the films, crystalline phases were clearly identified both on titanium in the as-received condition and anodised at 30 V. The spectrum corresponding to each surface condition were compared to those previously reported for anodic oxide films on titanium [39,42,66,74–76] (see Table 2). Raman spectra of anodic films on titanium are characterised by broad peaks with a shift respect of the powder samples [76–80] or even respect of TiO_2 sol–gel films.[81] The most intense Raman peak of anatase is reported for TiO_2 powder samples at 144–146 cm^{-1}. However, on anodised titanium, Sul *et al.* determined that anatase peak was at 150–153 cm^{-1},[39] whereas Liu *et al.* reported the anatase peak at 158 cm^{-1}.[66]

The micrograph corresponding to as-received titanium is presented in Fig. 4.a., along with the 3D representation of the spectra taken trough the line. Anatase peaks were detected, in a few points along the line. These results account the presence of isolated regions with crystalline order on the as-received titanium, in opposition to the reports of amorphous structure of native TiO_2.[39,60,82]

In Fig. 5, titanium anodised at 30 V micrograph and corresponding Raman spectra along a line are presented. The main anatase peak (146–151 cm^{-1}), together with some broad bands corresponding to the crystallographic phase, is presented on the line where the Raman spectra were taken. Additionally, some peaks of minor intensity assignable to rutile were detected in a few points.

The above results evidences that the films obtained at low potentials are non homogeneous and partially crystalline.

Chemical species on anodised titanium

Survey spectra of as-received and anodised titanium at different potentials are presented in Fig. 6. Peaks corresponding to C, O and Ti are characteristic of the as-received condition, with minor intensities of N and Ca peaks, attributed to impurities from the

UNCORRECTED

Copyright © 2012 John Wiley & Sons, Ltd.

Colour online, B&W in print

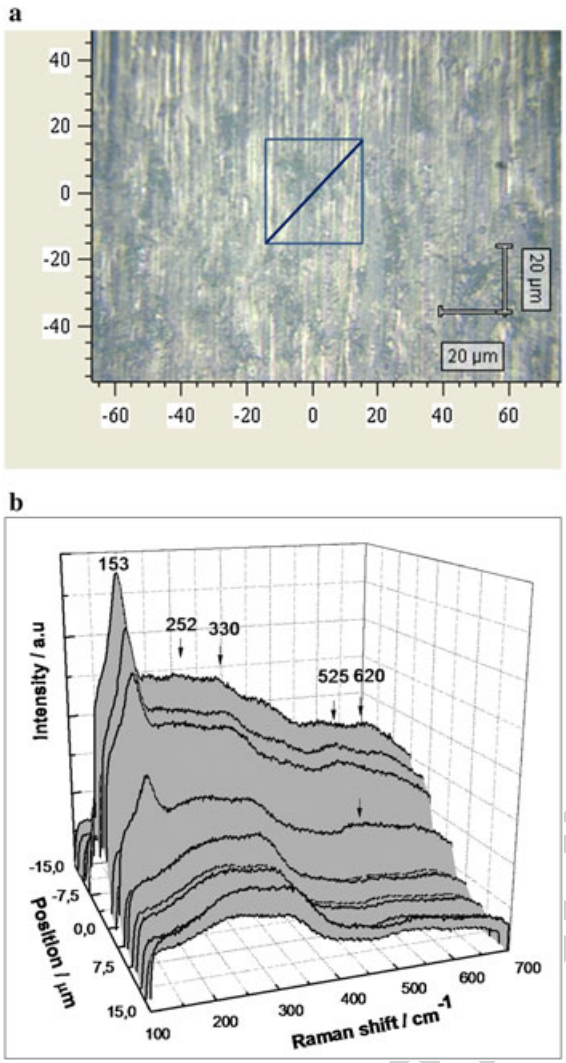

Figure 4. **a**. Optical micrograph of as-received titanium, with the line where the Raman spectra were taken. **b**. Raman spectra on different points along the line.

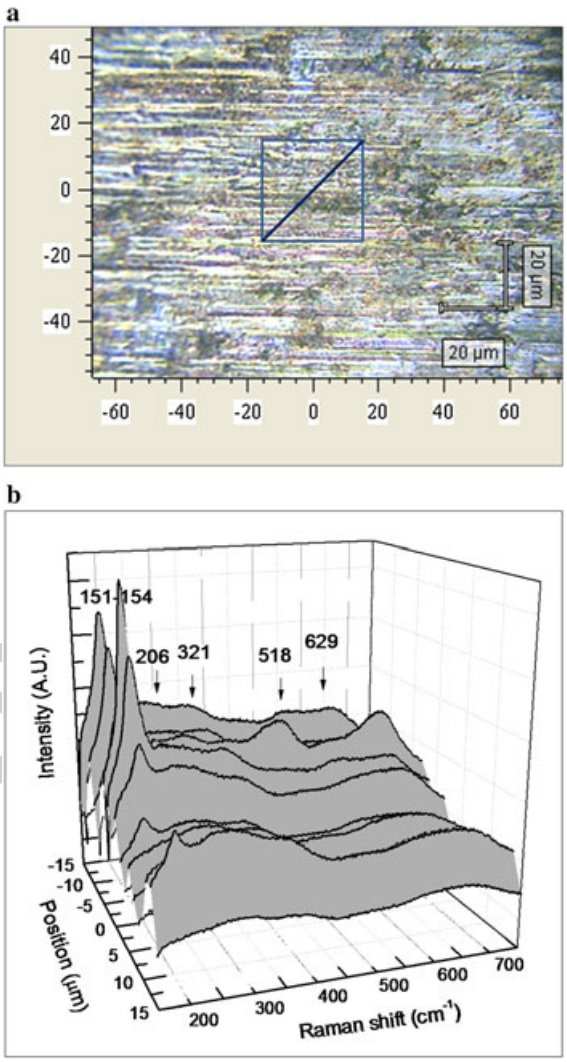

Figure 5. **a**. Optical micrograph of titanium anodised at 30 V, with the line where the Raman spectra were taken. **b**. Raman spectra on different points along the line.

Table 2. Raman peaks assignable to TiO_2 *Anatase* and *Rutile* peaks, with the peaks corresponding to titanium anodised at 30 V

Anatase				**Rutile**				**Anodic oxide**
Shibata and Zhu (1995)	Liu *et al.* (2009)	Sul *et al.* (2002)	Hardcastle *et al.* (2009)	Shibata and Zhu (1995)	Liu *et al.* (2009)	Sul *et al.* (2002)	Hardcastle *et al.* (2009)	
145		144–145	144			143		**150–153**
		197	197					**204–207**
				236		236	238	
								319–323
400	380–450	397–399	396					
				447	445	447	446	
515		515–516	514					**512–520**
					607	612	612	
			635					**624–632**
640	600–650	639–641						

UNCORRECTED

Copyright © 2012 John Wiley & Sons, Ltd.

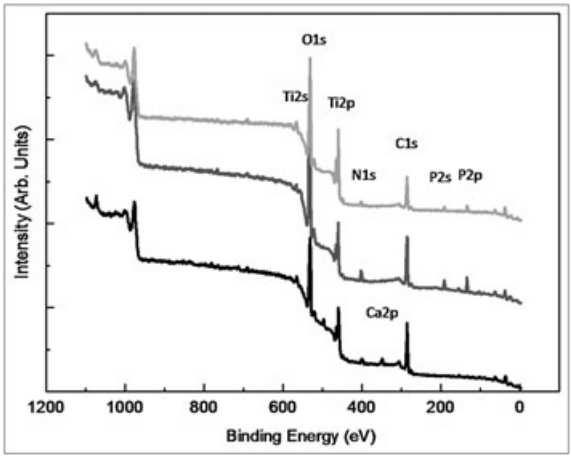

Figure 6. Survey spectra of Ti (–) as-received and anodised at (–) 12 V and (–) 30 V.

sheet lamination process.[83] On anodised samples, peaks corresponding to P2s and P2p are also present. The chemical shift on P2p spectrum (Fig. 7) may be related to the presence of pyrophosphates on the surface of the anodised samples.[84] Similar reports of P incorporated on anodic oxides surfaces during anodisation were previously reported from XPS and Auger spectroscopy results,[85–87] whereas with XRD, titanium phosphates were identified on anodic oxides growth in H_3PO_4 1 mol/l at potentials between 100 and 250 V.[51]

Many authors agree in the beneficial effect of the incorporation of phosphates to anodic surface oxides on titanium and some of its alloys to the *in vitro* capability of precipitation of bioactive Ca-P compounds during immersion in simulated body fluids.[5,88–90]

The multi-technique evaluation performed evidences of some improvement in surface characteristics when comparing the as-received titanium with the anodised at 30 V. Although the surface morphology in the micrometrical scale does not present modifications, as it was observed by SEM analysis, the topography of titanium oxide surface was modified by anodisation in the nanometrical range. Thus, an increase in roughness parameters was detected, which may be beneficial for the implant fixation.

Moreover, the crystalline phase present on titanium anodised at 30 V was those considered as more biocompatible, and also the incorporation of phosphate on the anodic film is presented as an improvement in the biocompatible characteristics of the oxide film obtained by anodisation.

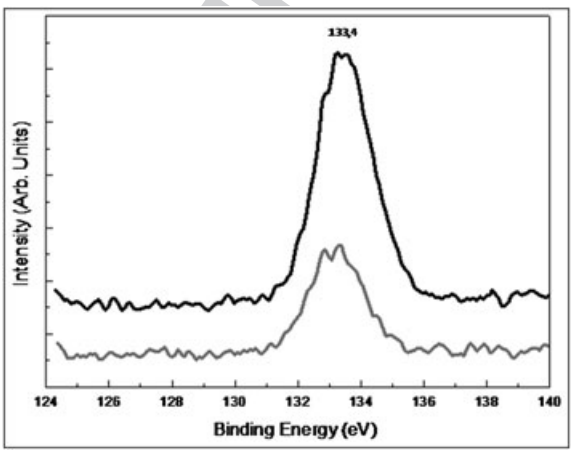

Figure 7. P 2p spectra for Ti anodised at (–) 30 V and (–) 12 V.

Electronic properties of the anodic films

Besides the topography and the chemical modification of titanium with different surface modification treatments, in recent articles, it is pointed out that the semiconducting characteristics of the surface oxide film on titanium may play a role in the *in vivo* behaviour of implants.[91] Titanium oxide films behave as n type semiconductors, as it was widely stated.[92–97] However, the electronic characteristics of these films are strongly influenced by the surface conditioning, even when native oxides are compared.[91]

The semiconductive behaviour of the films was evaluated by means of the Mott–Shottky model,[56] which describes a linear relationship between the space charge capacitance of the film and the applied potential (Eqn 1)).

$$\frac{1}{C_{sc}{}^2} = \frac{2}{qN_d\varepsilon\varepsilon_0}\left(V - V_{fb} - \frac{kT}{q}\right) \quad (1)$$

where C_{sc} is the capacitance of the space charge region, q is the charge of the charge carriers, N_d is the carrier number density (cm^{-3}), ε is the relative dielectric permittivity of the film, ε_0 is the permittivity of free space (8.85 × 10–14 F cm^{-1}), V is the applied potential, V_{fb} is the flat band potential, k is the Boltzman constant and T the absolute temperature. The sign of the slope in Eqn (1) indicates the type of semiconductor film present (n- or p-); the number density of charge carriers can be calculated from its value, and the intercept with the V axis at $1/C^2 = 0$ gives the flat band potential. In the absence of additional series components of the capacitance or when the semiconductor-solution interfacial capacitance is very large compared with C_{sc}, the space charge capacitance can be determined from the imaginary component of the impedance (Z″) at high frequencies according to:

$$Z'' = -\frac{1}{\omega A C_{SC}} \quad (2)$$

ω is the angular frequency and A is the electrode area. The semiconductor behaviour of the anodic oxide films was investigated from Mott–Schottky plots constructed using capacitance measurements at 1000 Hz for potentials between 0 and 3 V, which is a range wider than that usually investigated for titanium anodic oxide films. In Fig. 8, the Mott–Schottky plot corresponding to titanium anodic films obtained at different potentials is presented. The n type semiconductive behaviour is verified.

To determine the carrier number using Eqn (1), the permittivity of the anodic films has to be assumed. Shultze and Lorherengel in a review devoted to titanium oxide films reported a range of permittivity of TiO_2 from 3 to 104.[98] The permittivity of a material is related with its crystalline structure, and therefore the wide range takes into account the various crystalline phases of TiO_2 films and also the degree of crystallinity. In this work, despite the presence of crystalline order in some regions of the surface films, the degree of crystallinity is low, and the permittivity of anatase ($\varepsilon = 30$) or rutile ($\varepsilon = 100$) are not adequate.[99] The permittivity of anodic films was determined by other authors from impedance spectroscopy, ellipsometry or capacitance determinations, and values between 30 and 65 were obtained.[42,99–102] In all these experimental determinations, besides the growing conditions of the films, some starting assumptions are needed in the result analysis (film structure, density, refractive index, thickness, among others) that have influence

UNCORRECTED PROOF

Copyright © 2012 John Wiley & Sons, Ltd.

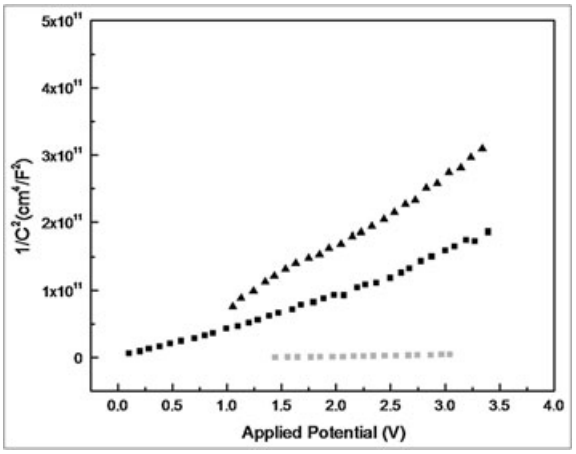

Figure 8. Mott–Schottky plots of titanium (▩) as received and anodised at (■) 12 V and (▲) 30 V in 1 mol/l phosphoric acid.

on the outcoming value. Taking these matters in mind, a value of $\varepsilon = 46$ was assumed, according to that reported by Badekas and Panagopoulos for anodic oxide films growth on titanium in comparable conditions of potential range and type of electrolyte with the ones used in this work.[52]

The carrier numbers obtained using Eqn 2 are presented in Fig. 9 as a function of the growing potential. The results are in good agreement with those reported by other authors (between 10^{18} and 10^{23} cm^{-3}) and also the decrease of the carrier number when increasing anodising potential (and therefore anodic film thickness).[91,103,104] Moreover, the Nd values obtained are in the range studied by Petersson *et al.* as adequate for titanium dental implants.[91]

EIS

EIS results corresponding to titanium as-received and anodised at different potentials are presented in Fig. 10. The impedance response for titanium in the different surface conditions evaluated showed a typical capacitive behaviour, characterised by a wide range of frequencies for which the phase angle remains close to −90º. For all the conditions investigated, the slope of

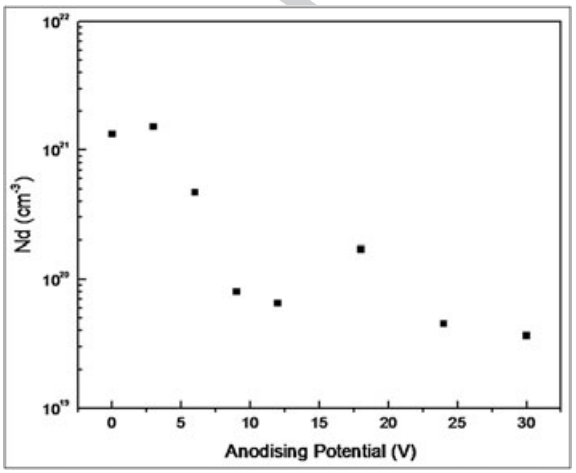

Figure 9. Dependence of the charge carrier number density on anodising potential determined from the Mott–Shottky analysis.

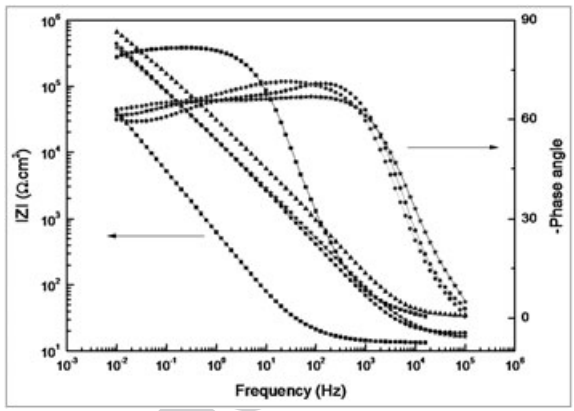

Figure 10. Bode plots of the as-received and anodised titanium at different potentials in 1.0 mol dm^{-3} phosphoric acid: Anodising potentials: 0 V (■), 12V (●), 24 V (▲) and 30 V (*). Solid lines show the equivalent circuit fitting.

the line in the Bode plot of the impedance modulus *versus* frequency differs, however, from unity, an indication of a non-ideal capacitor.[114] This behaviour is characteristic of passive films and has been observed for valve metals native oxide films.[96,113] The impedance modulus also increases by increasing the anodising potential, indicating the formation of a more resistive film. An increase in the impedance modulus of one order of magnitude between the anodic oxides and the as-received surface takes into account the presence of the anodic film, which enhances the barrier effect.[105,106]

The circuital fitting of EIS results of titanium oxide films has been extensively discussed in literature both related to native oxides and anodic films.[42,65,97,107–110] The simplest circuit used to describe a dense oxide film on a metallic substrate is that composed by an ideal capacitor (C_{ox}) with a parallel resistance (R_{ox}), in series with the resistance corresponding to the electrolyte.[96,111] The circuit was used by Badawy *et al.* to describe the behaviour of native oxides on tantalum and titanium.[112] They found that an accurate description of tantalum native oxide was possible, whereas it was not appropriated to describe titanium native oxide.

The circuital model used to represent the native oxide is presented in Fig. 11.a. This circuit includes a constant phase

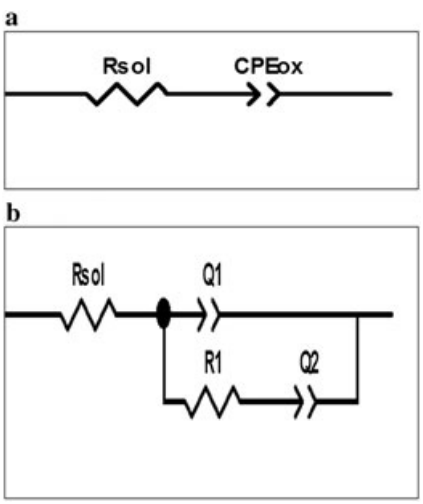

Figure 11. Equivalent circuits employed for data fitting: **a**. as-received titanium **b**. anodised titanium.

UNCORRECTED PROOF

Copyright © 2012 John Wiley & Sons, Ltd.

element (CPE) instead of a capacitor to describe the oxide layer, where the electrolyte resistance (Rsol) is in series with the interfacial impedance. The impedance of a CPE is given by:

$$Z_{CPE} = 1/Q(j\omega)^{\alpha} \quad (3)$$

where Q is a parameter independent of frequency, and α is a coefficient associated with system homogeneity [62,89–93]. When $\alpha = 1$, Q has units of capacitance (F cm^{-2}) and represents the capacitance of the interface. When $\alpha < 1$, the system shows a behaviour that can be attributed to surface heterogeneity or to a distribution of time constants, and in this case, Q has units of $s^{\alpha}\ \Omega^{-1}\ cm^{-2}$.

The behaviour represented by the circuit 11.a. may be related to the transition between a porous surface layer and a capacitive film, where the response of the metal/film system is dominated by the charge transfer, thus leading to the presence of a single time constant.[62,113] The CPE takes into account the distribution of relaxation times of the system, often attributed to the presence of surface defects or inhomogeneities. The circuit proposed for the native oxide has been previously used to describe native oxides on polished and electropolished zirconium,[114] instead of the circuit proposed by Harrison and Williams, because the values corresponding to Rox tend to infinite values, losing its physical meaning in the description of the structure of the film.

The EIS response for the anodic oxides is more complex. Two time constants are present, corresponding to a two-layer model of the anodic oxide structure (Fig. 11.b.). The inner layer dominates the EIS response in high frequencies; meanwhile an outer porous layer dominates the low frequencies impedance. This two-layered model has been extensively discussed in the literature related to anodic titanium, using as in other valve metals, different configurations of resistances and capacitors or CPEs.[42,66,100] A possible reason for the numerous models proposed for titanium anodic oxides may be attributed to the differences in growth conditions, and therefore, the actual structure of the films. Moreover, the EIS response is dependent of the electrolyte used, since many surface interactions may occur during the immersion (absorption or adsorption of species, thickening of the film, dissolution, precipitation of compounds from the electrolyte on the surface, among others). Finally, the use of a circuit is not unique, since several circuital elements arrangements may lead to identical mathematical behaviour that results in a good correlation with the experimental EIS result.[115]

In Fig. 11.b., Q1 corresponds to the inner pseudocapacitance, and Q2 is related to the dispersion in frequencies due to the porous outer layer, describing the processes occurring inside the pores. Q2 with α values close to 0.5 is used to model the increase of the ionic conductivity due to corrosion processes and the increase of diffusivity in the pores. The decrease in α when increasing the anodising potential indicates the increase in the diffusion process in the porous outer layer. R1 in the circuit is related to the charge transfer and the resistance to the ionic conductivity. The increment of R1 along with the decrease in Q1 when increasing the anodising potential describes the effect of the increasing thickness of the anodic films.

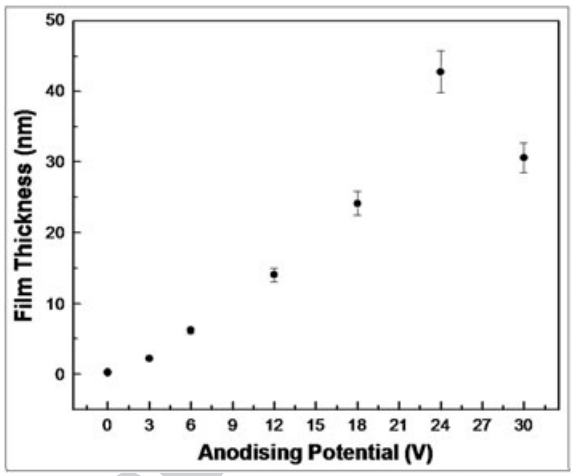

Figure 12. Anodic film thickness of anodised titanium samples calculated from the Brug model.

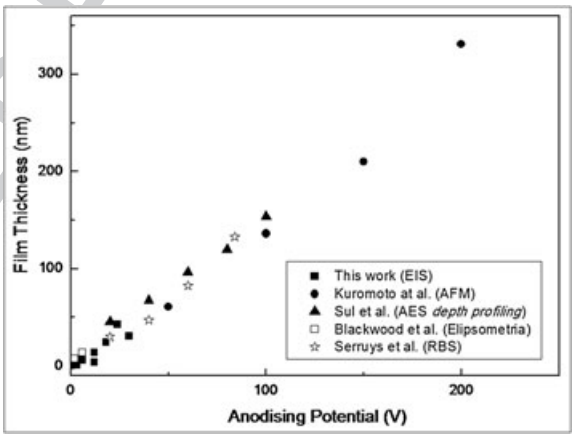

Figure 13. Anodic film thickness obtained in this work compared with previously published results.

Thickness of the anodic surface films

Thickness determinations from EIS results have been previously reported for anodic films on titanium. However, the validity of the method remains controversial. Blackwood postulated that due to the influence of the space charge on EIS response, the capacitance is dominated by this region and therefore the

Table 3. Detail of the anodising conditions used to obtain films compared in Fig. 13

Anodising process	Electrolyte	Thickness determination	Ref.
Potentiostatic 60 min.	H_3PO_4 1 mol/l.	Electrochemical Impedance Spectroscopy	**Este trabajo**
Potentiostatic 1 min.	H_3PO_4 1,4 mol/l.	Contact mode AFM	**Kuromoto *et al*. (2007)**
Galvanostatic 5 mA/cm^2	H_3PO_4 1 mol/l.	AES *depth profiling*	**Sul y col (2002)**
Potentiodinamic 100 mV/seg	H_2SO_4 3 mol/l.	Elipsometry	**Blackwood y col. (1989)**
Galvanostatic 12 mA/cm^2	H_2SO_4 1 mol/l.	Rutherford Backscatter Spectroscopy	**Serruys y col. (1993)**

UNCORRECTED PROOF

Copyright © 2012 John Wiley & Sons, Ltd.

thickness of this region instead of the actual film thickness is evaluated.[96] Recently, Peterson *et al*. determined experimentally that the space charge has not major effect on EIS response on native and anodic films, and then the determination of the film thickness may be calculated from EIS results when an adequate circuit is used to fit the experimental results.[91] In numerous works, the film thickness is determined assuming an ideal capacitive behaviour of the films, and using the parallel plate capacitor equation,[52,65,91] or when considering a CPE, taking the pseudocapacitive parameter as an ideal capacitor.[29]

Previously, the determination of the film thickness of the films of anodic oxides when EIS results include CPEs was evaluated in zirconium anodic films, and the Brug and Hsu and Mansfeld approaches were discussed.[118,119] It was concluded that when the CPE behaviour is due to inhomogeneities in the properties of the electrode surface a parallel combination of local impedances is considered, and the Brug *et al*. relation between circuital parameters and the effective capacitance (C_{eff}) associated with the *CPE* element may be adequate:

$$C_{eff} = Q^{1/\alpha}\left(R_{sol}{}^{-1} + R_t{}^{-1}\right)^{(1-\alpha)/\alpha} \quad (4)$$

In this relation, R_{sol} is the electrolyte ohmic resistance, R_t relates to the charge transfer resistance associated with the kinetics of oxide growth and Q is the pseudocapacitance of the film.

The oxide thickness can be estimated from C_{eff}, assuming that the film behaves as a pure capacitor. In this case, the capacitance is given by:

$$C_{eff} = \varepsilon\varepsilon_0 A/d_{eff} \quad (5)$$

where d_{eff} is the film thickness. Figure 10 shows the dependence of film thickness on growth potential taking $\varepsilon = 46$ for TiO_2.[52] Regardless of the complexity of the film structure, the EIS results can be conveniently employed to estimate film thickness through the measured values of C_{eff}. A linear dependence of the calculated thickness on anodising potential is observed for most of the potential range, as expected if the constant field approximation for film growth is applicable,[120] which is indeed the case here (Fig. 12). Moreover, as it is evidenced in Fig. 13 and Table 3, the thickness values obtained in this work from EIS results, using the Brug equation to extract the effective capacitance of the film are in good agreement with those obtained for other authors using different experimental techniques.

The electrochemical studies performed evidence that the anodisation in phosphoric acid on titanium allows the increase of a barrier film with electronic properties compatible with the biological media. Further studies in simulated body fluid solution are needed in order to evaluate the stability of the films obtained *in vitro*.

Conclusions

Adequate techniques were selected and critically compared with previous results in literature, in order to present an accurate comprehension of the surface modification performed with the anodisation process at low potentials with the aim of induce bioactivity with increasing corrosion resistance *in vitro*.

Beneficial characteristics for permanent implant Ti implants, as the presence of anatase on the anodised surface, and phosphate incorporation from the electrolyte were determined. Carrier number in the range reported from other titanium implant materials was also verified, showing a decrease of the carrier number when increasing anodising potential,

From the circuital fitting of EIS results and according to the Brug model, film thickness was estimated, and the values obtained were in good agreement with those available from independent techniques, thus validating the estimation. The native oxide is present in the as-received condition, increasing thickness with anodising potential. The barrier effect is also enhanced with the increase of the thickness.

Further *in vitro* electrochemical and immersion tests in SBF results will correlate the characteristics determined in this work with the response in a simulated biological media.

References

[1] G. Mendonça, D. B. S. Mendonça, F. J. L. Aragão, L. F. Cooper, *Biomaterials* **2008**, *29*, 3822.
[2] J. E. Davies, *Biomaterials* **2007**, *28*, 5058.
[3] A. L. Oliveira, J. F. Mano, R. L. Reis, *Curr Opin Solid ST M* **2003**. *7*, 309.
[4] F. Barrere, M. M. E. Snel, C. A. van Blitterswijk, K. de Groot, P. Layrolle, *Biomaterials* **2004**, *25*, 2901.
[5] Y. T. Sul, *Biomaterials* **2003**, *24*, 3893.
[6] O. Suzuki, S. Kamakura, T. Katagiri, M. Nakamura, B. Zhao, Y. Honda, R. Kamijo, *Biomaterials* **2006**, *27*, 2671.
[7] B. Feng, J. Weng, B. C. Yang, S. X. Qu, X. D. Zhang, *Biomaterials* **2004**, *25*, 3421.
[8] K. C. Baker, M. A. Anderson, S. A. Oehlke, A. I. Astashkina, D. C. Haikio, J. Drelich, S. W. Donahue, *Mater Sci Eng* **2006**, *C26*, 1351.
[9] R. M. Souto, M. M. Laz, R. L. Reis, *Biomaterials* **2003**, *24*, 4213.
[10] C. Ergun, R. Doremus, W. Lanford, *J biomed Mat Res A* **2003**, *65*, 336.
[11] C. Berbecaru, H. V. Alexandru, G. E. Stan, D. A. Marcov, I. Pasuk, A. Ianculescu, *Mat Sci Eng* **2010**, *B169*, 101.
[12] J.-H. Park, Y.-K. Lee, K.-M. Kim, K.-N. Kim, *Surf Coat Tech* **2005**, *195*, 252.
[13] J.-H. Park, D.-Y. Lee, K.-T. Oh, Y.-K. Lee, K.-M. Kim, K.-N. Kim, *Mat Lett* **2006**, *60*, 2573.
[14] A. Raknagarm, Y. Mutoh, *Mat Sci Eng* **2009**, *C29*, 275.
[15] P. Ducheyne, S. Radin, M. Heughebaert, J. C. Heughebaert, *Biomaterials* **1990**, *11*, 244.
[16] A. Balamurugan, G. Balossier, J. Michel, J. M. F. Ferreira, *Electrochim. Acta* **2009**, *54*, 1192.
[17] J.-C. Huang, Y.-J. Ni, Z.-C. Wang, *Surf Coat Tech* **2010**, *204*, 3387.
[18] Y.-S. Hsu, E. Chang, H.-S. Liu, *Ceram Inte* **1998**, *24*, 7.
[19] P. Habibovic, F. Barrére, C. A. van Blitterswijk, K. de Groot, P. Layrolle, *J Am Cer Soc* **2002**, *85*, 517.
[20] J.-S. Oh, Y.-H. Lee, B.-A. Kang, S.-B. Kim, K.-S. Hwang, *Ceram Int* **2003**, *29*, 847.
[21] L. Jonasova, F. A. Muller, A. Helebrant, J. Strnad, P. Greil, *Biomaterials* **2004**, *25*, 1187.
[22] H. S. Ryu, W.-H. Song, S.-H. Hong, *Surf Coat Tech* **2008**, *202*, 1853.
[23] C.-M. Lin, S.-K. Yen, *Mat Sci Eng* **2006**, *C26*, 54.
[24] H. M. Kim, F. Miyaji, T. Kokubo, T. Nakamura, *J Biomed Mat Res* **1996**, *32*, 409.
[25] C. X. Wang, M. Wang, X. Zhou, *Biomaterials* **2003**, *24*, 3069.
[26] X. J. Wang, Y. C. Li, J. G. Lin, Y. Yamada, P. D. Hodgson, C. E. Wen, *Acta Biomater.* **2008**, *4*, 1530.
[27] J. Faure, A. Balamurugan, H. Benhayoune, P. Torres, G. Balossier, J. M. F. Ferreira, *Mat Sci Eng* **2009**, *C29*, 1252-1257.
[28] M. Uchida, H.-M. Kim, F. Miyaji, T. Kokubo, T. Nakamura, *Biomaterials* **2002**, *23*, 313.
[29] M. Aziz-Kerrzo, K. G. Conroy, A. M. Fenelon, S. T. Farell, C. B. Breslin, *Biomaterials* **2001**, *22*, 1531.
[30] M. Karthega, N. Rajendran, *Appl. Surf. Sci.* **2010**, *256*, 2176.
[31] M. Karthega, S. Nagarajan, N. Rajendran, *Electrochim. Acta* **2010**, *55*, 2201.
[32] J.-W. Park, Y.-J. Kim, J.-H. Jang, T.-G. Kwon, Y.-C. Bae, J.-Y. Suh, *Acta Biomater.* **2010**, *6*, 1661.
[33] X. Lu, Z. Zhao, Y. Leng, *Mat Sci Eng* **2007**, *C27*, 700.
[34] M. Browne, P. J. Gregson, *Biomaterials* **2000**, *21*, 385-392.
[35] V. Barranco, E. Onofre, M. L. Escudero, M. C. García-Alonso, *Surf Coat Tech* **2010**, *204*, 3783.
[36] S. Kumar, T. S. N. Sankara Narayanan, S. Sundara Raman, S. K. Seshadri, *Mat Sci Eng* **2010**, *C30*, 921.

UNCORRECTED PROOF

Copyright © 2012 John Wiley & Sons, Ltd.

[37] J. Hall, J. Lausmaa, *Appl Osseointegration Research* **2000**, *1*, 1.
[38] Y.-T. Sul, C. B. Johansson, Y. Jeong, T. Albrektsson, *Med. Eng. Phys.* **2001**, *23*, 329.
[39] Y.-T. Sul, C. B. Johansson, S. Petronis, A. Krozer, Y. Jeong, A. Wennerberg, T. Albrektsson, *Biomaterials* **2002**, *23*, 491.
[40] B. Yang, M. Uchida, H.-M. Kim, X. Zhang, T. Kokubo, *Biomaterials* **2004**, *25*, 1003.
[41] H.-J. Oh, J.-H. Lee, Y. Jeong, Y.-J. Kim, C.-S. Chi, *Surf Coat Tech* **2005**, *198*, 247.
[42] C. Jaeggi, P. Kern, J. Michler, T. Zehnder, H. Siegenthaler, *Surf Coat Tech* **2005**, *200*, 1913.
[43] B. S. Ng, I. Annergren, A. M. Soutar, K. A. Khora, A. E. W. Jarfors, *Biomaterials* **2005**, *26*, 1087.
[44] W. Chrzanowski, J. Szewczenko, J. Tyrlik-Held, J. Marciniak, J. Zak, *J Mat Proc Tech* **2005**, *162-163*, 163.
[45] N. K. Kuromoto, R. A. Simão, G. A. Soares, *Mater. Charact.* **2007**, *58*, 114.
[46] J.-H. Liu, J.-L. Yi, S.-M. Li, M. Yu, Y.-Z. Xu, *Int J Min Met Mater* **2009**, *16*, 96.
[47] X. Cui, H.-M. Kim, M. Kawashita, L. Wang, T. Xiong, T. Kokubo, T. Nakamura, *Dent. Mater.* **2009**, *25*, 80.
[48] J. L. Trompette, L. Massot, L. Arurault, S. Fontorbes, *Corros. Sci.* **2011**, *53*, 1262.
[49] W. Simka, A. Sadkowski, M. Warczak, A. Iwaniak, G. Dercz, J. Michalska, A. Maciej, *Electrochim. Acta* **2011**, *56*, 8962.
[50] R. Narayanan, S. K. Sechadri, *Corros. Sci.* **2007**, *49*, 542.
[51] Y. L. Park, K. H. Shin, H. J. Song, *Appl. Surf. Sci.* **2007**, *253*, 6013.
[52] H. Badekas, C. Panagopoulos, *Surf Coat Tech* **1987**, *31*, 381.
[53] J. Proost, J. F. Vanhumbeek, Q. Van Overmeere, *Electrochim. Acta* **2009**, *55*, 350.
[54] A. Afshar, M. R. Vaezi, *Surf Coat Tech* **2004**, *186*, 398.
[55] A. Gomez Sanchez, W. Schreiner, G. Duffó, S. Ceré, *Appl. Surf. Sci.* **2011**, *257*, 6397.
[56] A. W. Bott, *Curr Separations* **1998**, *17*, 87.
[57] Zplot for Windows, Scribner Ass. Inc., Southern Pines, NC, **1998**.
[58] J.-L. Delplancke, M. Degrez, A. Fontana, R. Winand, *Surf Tech* **1982**, *16*, 153.
[59] A. Perez del Pino, J. M. Fernandez Pradas, P. Serra, J. L. Morenza, *Surf Coat Tech* **2004**, *187*, 106.
[60] S. A. Fadl-allah, Q. Mohsen, *Applied Surf Sci* **2010**, *256*, 5849.
[61] Ch. Jung Ch, Surface Treatment of Titanium, The Tribology of Precision - Swiss Tribology Meeting, SBB Centre Löwenberg in Murten, Switzerland, **2007**.
[62] H.-J. Song, S.-H. Park, S.-H. Jeong, Y.-J. Park, *J Mater Proc Tech* **2009**, *209*, 864.
[63] B. Yang, M. Uchida, H.-M. Kim, X. Zhang, T. Kokubo, *Biomaterials* **2004** *25*, 1003.
[64] U. Diebold, *Surf Sci Reports* **2003**, *48*, 53.
[65] J. R. Birch, T. D. Burleigh, *Corrosion* **2000**, *56*, 1233.
[66] T. Shibata, Y.-C. Zhu, *Corros. Sci.* **1995**, *37*, 133.
[67] J. Yahalom, J. Zahavi, *Electrochim. Acta* **1970**, *15*, 1429.
[68] J. S. L. Leach, B. R. Pearson, *Corros. Sci.* **1988**, *28*, 43.
[69] H. Habazaki, M. Uozumi, H. Konno, K. Shimizu, P. Skeldon, G. E. Thompson, *Corros. Sci.* **2003**, *45*, 2063.
[70] M. R. Kozlowski, P. S. Tyler, W. H. Smyrl, R. T. Atanasoski, *Surf. Sci.* **1988**, *194*, 505.
[71] J.-L. Delplancke, A. Garnier, Y. Massiani, R. Winard, *Electrochim. Acta* **1994**, *39*, 1281.
[72] H.-J. Song, M.-K. Kim, G.-C. Jung, M.-S. Vang, Y.-J. Park, *Surf Coat Tech* **2007**, *201*, 8738.
[73] J. Löberg, University of Gothenburg, Ph D Thesis, **2011**.
[74] J. Zhao, X. Wang, R. Chen, L. Li, *Solid State Commun* **2005**, *134*, 705.
[75] F. D. Hardcastle, H. Ishihara, R. Sharma, A. S. Biris, en Proc. Electrostatic Society of America Annual Meeting, Boston, **2009**.
[76] H. Berger, H. Tang, F. Lévy, *J Cryst Growth* **1993**, *130*, 108.
[77] H. C. Choi, Y. M. Jung, S. B. Kim, *Vib Spectrosc* **2005**, *37*, 33.
[78] L. Kavan, J. Rathousky, M. Grätzel, V. Schklover, A. Zukal, *Micropor Mesopor Mat* **2001**, *44-45*, 653.
[79] K.-R. Zhu, M.-S. Zhang, Q. Chen, Z. Yin, *Phys Lett A* **2005**, *340*, 220.
[80] S. J. Rigby, A. H. R. Al-Obaidi, S.-K. Lee, D. McStay, P. K. L. Robertson, *App Surf Sci* **2006**, *252*, 7948.
[81] Y. Djaoued, K. Ozga, A. Wojciechowski, A. H. Reshak, J. Robichaud, I. V. Kityk, *J Alloy Compd* **2010**, *490*, 576-582.
[82] A. G. Mantzila, M. I. Prodromidis, *Electrochim. Acta* **2006**, *51*, 3537.
[83] J. Lausmaa, *J Electron Spectrosc* **1996**, *81*, 343.
[84] J. F. Moulder, W. F. Stickle, P. E. Sobol , K. D. Bomben, Handbook of X-ray photoelectron spatroscopy, Physical Electronics Inc, Eden Praire, Minnesota, **1995**.
[85] J. Lausmaa, B. Kasemo, H. Mattson, *Appl. Surf. Sci.* **1990**, *44*, 133.
[86] J. Lausmaa, B. Kasemo, H. Mattson, H. Odelius, *Appl. Surf. Sci.* **1990**, *45*, 189.
[87] C. E. B. Marino, P. A. P. Nascente, S. R. Biaggio, R. C. Rocha-Filho, N. Bocchi, *Thin Solid Films* **2004**, *468*, 109.
[88] T. Hanawa, M. Kaga, Y. Itoh, T. Echizenya, H. Oguchi, M. Ota, *Biomaterials* **1992**, *13*, 20.
[89] J.-H. Lee, S.-E. Kim, Y.-J. Kim, C.-S. Chi, H.-J. Oh, *Mater. Chem. Phys.* **2006**, *98*, 39.
[90] L. A. de Sena, N. C. C. Rocha, M. C. Andrade, G. A. Soares, *Surf Coat Tech* **2003**, *166*, 254.
[91] I. Petersson, J. E. L. Löberg, A. S. Fredriksson, E. K. Ahlberg, *Biomaterials* **2009**, *30*, 4471.
[92] D. J. Blackwood, L. M. Peter, D. E. Williams, *Electrochim. Acta* **1988**, *33*, 1143.
[93] D. J. Blackwood, R. Greef, L. M. Peter, *Electrochim. Acta* **1989**, *34*, 875.
[94] D. J. Blackwood, L. M. Peter, *Electrochim. Acta* **1989**, *34*, 1505.
[95] T. Ohtsuka, T. Ohtsuki, *Corros. Sci.* **1998**, *40*, 951.
[96] D. J. Blackwood, *Electrochim. Acta* **2000**, *46*, 563.
[97] P. Bourdet, F. Vacandio, L. Argème, S. Rossi, Y. Massiani, *Thin Solid Films* **2005**, *483*, 205.
[98] J. W. Schultze, M. M. Lohrengel, *Electrochim. Acta* **2000**, *45*, 2499.
[99] M. Dolata, P. Kedzierzawski, J. Augustynski, *Electrochim. Acta* **1996**, *41*, 1287.
[100] J. Marsh, D. Gorse, *Electrochim. Acta* **1998**, *43*, 659.
[101] W. Wilhelmsen, T. Hurlen, *Electrochim. Acta* **1987**, *32*, 85.
[102] T. Hurlen, S. Hornkjol, *Electrochima Acta* **1991**, *36*, 189.
[103] A. M. Schmidt, D. S. Azambuja, E. M. A. Martini, *Corros. Sci.* **2006**, *48*, 2901.
[104] N. Ibris, J. C. Mirza Rosca, *J. Electroanal. Chem.* **2002**, *526*, 53.
[105] V. Brunetti, M. Lopez teijelo, *J. Electroanal. Chem.* **2008**, *613*, 16.
[106] A. Cremasco, W. R. Osório, C. M. A. Freire, A. Garcia, R. Caram, *Electrochim. Acta* **2008**, *53*, 4867.
[107] J. Pan, D. Thierry, C. Leygraf, *J Biomed Mat Res* **1994**, *28*, 113.
[108] G. Nogami, Y. Ogawa, Y. Nishiyama, *J. Electrochem. Soc.* **1988**, *135*, 3008.
[109] A. Norlin, J. Pan, C. Leygraf, *Biomolec Eng* **2002**, *19*, 67.
[110] N. T. C. Oliveira, S. R. Biaggio, S. Piazza, C. Sunseri, F. Di Quarto, *Electrochim. Acta* **2004**, *49*, 4563.
[111] W. Simons, L. Pauwels, A. Hubin, *Electrochim. Acta* **2002**, *47*, 2169.
[112] J. A. Harrison, D. E. Williams, *Electrochim. Acta* **1982**, *27*, 891.
[113] W. A. Badawy, S. S. Elegamy, K. M. Ismail, *Br Corros J* **1993**, *28*, 133.
[114] A. Conde, J. J. de Damborenea, *Corros. Sci.* **2002**, *44*, 1555.
[115] T. Pauporté, J. Finne, *J Appl Elctrochem* **2006**, *36*, 33.
[116] J. R. Macdonald, Impedance spectroscopy emphasizing solid materials and systems, John Wiley & Sons, New York, **1987**.
[117] A. Gomez Sanchez, Universidad Nacional de General San Martín, Argentina. PhD thesis, **2011**.
[118] G. J. Brug, A. L. G. Van Den Eeden, M. Sluyters-Rehbach, J. H. Sluyters, *J. Electroanal. Chem.* **1984**, *176*, 275.
[119] C. S. Hsu, F. Mansfeld, *Corrosion* **2001**, *57*, 747.
[120] N. Sato, *Corros. Sci.* **1990**, *31*, 1.

UNCORRECTED PROOF

Copyright © 2012 John Wiley & Sons, Ltd.

Author Query Form

Journal: Surface and Interface Analysis

Article: sia_5210

Dear Author,

During the copyediting of your paper, the following queries arose. Please respond to these by annotating your proofs with the necessary changes/additions.

- If you intend to annotate your proof electronically, please refer to the E-annotation guidelines.
- If you intend to annotate your proof by means of hard-copy mark-up, please refer to the proof mark-up symbols guidelines. If manually writing corrections on your proof and returning it by fax, do not write too close to the edge of the paper. Please remember that illegible mark-ups may delay publication.

Whether you opt for hard-copy or electronic annotation of your proofs, we recommend that you provide additional clarification of answers to queries by entering your answers on the query sheet, in addition to the text mark-up.

Query No.	Query	Remark
Q1	AUTHOR: Please check this presentation if correct.	
Q2	AUTHOR: Reference “63” has not cited in the text. Please indicate where it should be cited; or delete from the reference list and renumber the references in the text and reference list.	
Q3	AUTHOR: Reference “116” has not cited in the text. Please indicate where it should be cited; or delete from the reference list and renumber the references in the text and reference list.	
Q4	AUTHOR: Reference “117” has not cited in the text. Please indicate where it should be cited; or delete from the reference list and renumber the references in the text and reference list.	
Q5	AUTHOR: Figure(s) 4 and 5 has been supplied in colour. Academic authors receive one page of colour in print free of charge where colour is justified to the journal editor. There is a charge of £350 for the second page and £150 per page for page(s) 5. Additional colour costs available on application. Industrial and government authors do not receive free colour. Please confirm if this figure is to be reproduced in (a) colour in print, (b) colour online only (at no charge to author) or (c) black and white. Colour will be invoiced when article is published in print. Also please note that for the option ‘‘(b) colour online only (at no charge to author)’’ could you kindly identify andmake necessary text amendments thatmay need to bemade in the caption or text with regard to this change.	
Q6	Author: As per style sheet Abstract should be in one paragraph.	

WILEY-BLACKWELL

USING e-ANNOTATION TOOLS FOR ELECTRONIC PROOF CORRECTION

Required software to e-Annotate PDFs: Adobe Acrobat Professional or Adobe Reader (version 7.0 or above). (Note that this document uses screenshots from Adobe Reader X)
The latest version of Acrobat Reader can be downloaded for free at: http://get.adobe.com/uk/reader/

Once you have Acrobat Reader open on your computer, click on the Comment tab at the right of the toolbar:

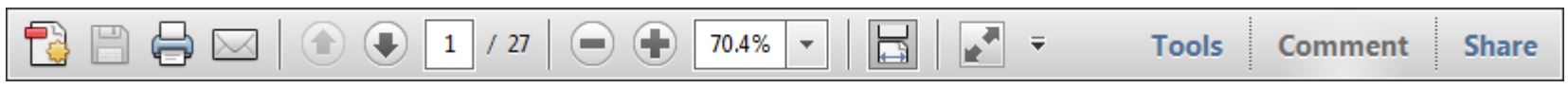

This will open up a panel down the right side of the document. The majority of tools you will use for annotating your proof will be in the Annotations section, pictured opposite. We've picked out some of these tools below:

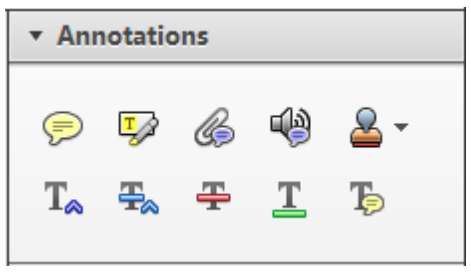

1. Replace (Ins) Tool – for replacing text.

Strikes a line through text and opens up a text box where replacement text can be entered.

How to use it

- Highlight a word or sentence.
- Click on the Replace (Ins) icon in the Annotations section.
- Type the replacement text into the blue box that appears.

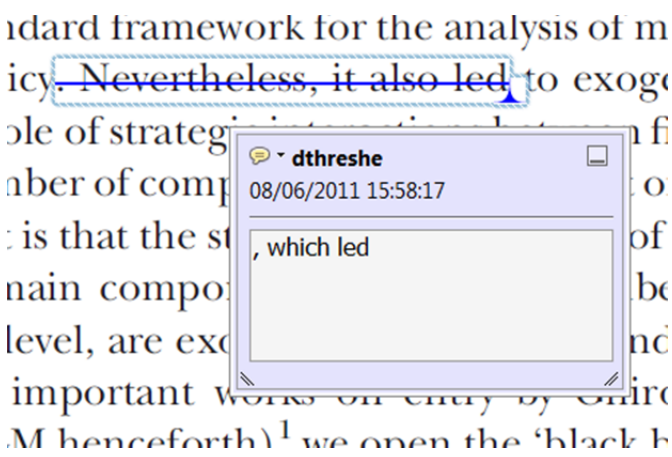

2. Strikethrough (Del) Tool – for deleting text.

Strikes a red line through text that is to be deleted.

How to use it

- Highlight a word or sentence.
- Click on the Strikethrough (Del) icon in the Annotations section.

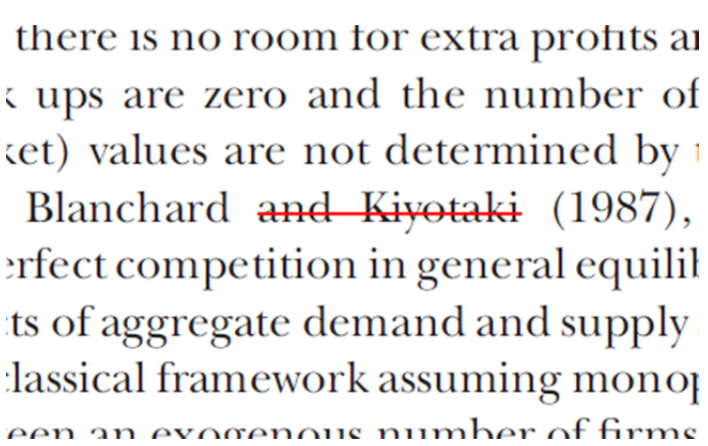

3. Add note to text Tool – for highlighting a section to be changed to bold or italic.

Highlights text in yellow and opens up a text box where comments can be entered.

How to use it

- Highlight the relevant section of text.
- Click on the Add note to text icon in the Annotations section.
- Type instruction on what should be changed regarding the text into the yellow box that appears.

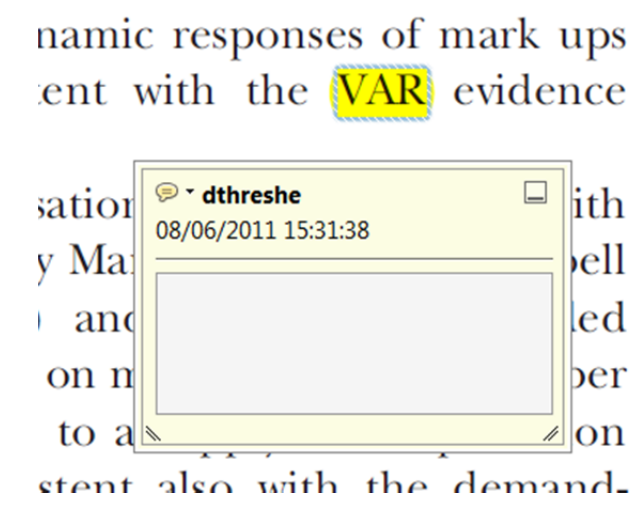

4. Add sticky note Tool – for making notes at specific points in the text.

Marks a point in the proof where a comment needs to be highlighted.

How to use it

- Click on the Add sticky note icon in the Annotations section.
- Click at the point in the proof where the comment should be inserted.
- Type the comment into the yellow box that appears.

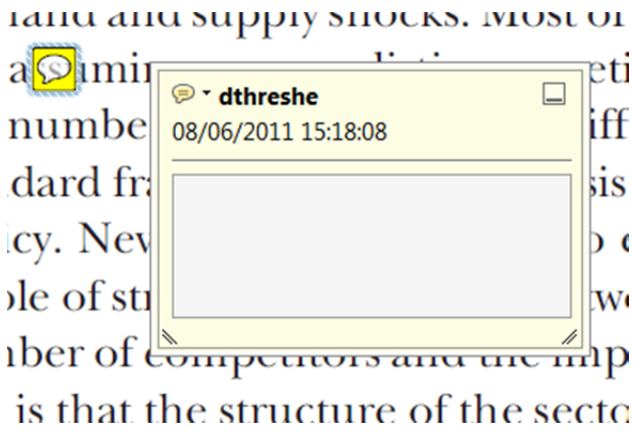

WILEY-BLACKWELL

USING e-ANNOTATION TOOLS FOR ELECTRONIC PROOF CORRECTION

5. Attach File Tool – for inserting large amounts of text or replacement figures.

Inserts an icon linking to the attached file in the appropriate pace in the text.

How to use it

- Click on the Attach File icon in the Annotations section.
- Click on the proof to where you'd like the attached file to be linked.
- Select the file to be attached from your computer or network.
- Select the colour and type of icon that will appear in the proof. Click OK.

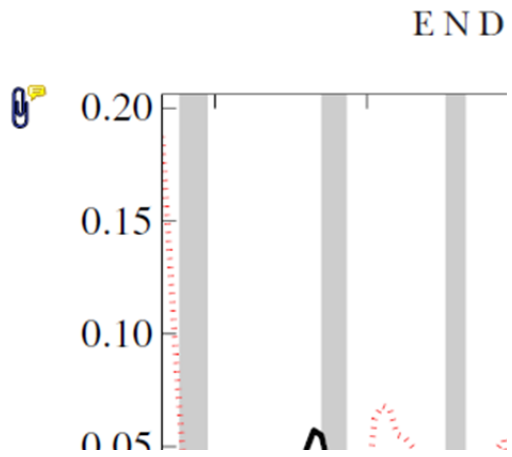

6. Add stamp Tool – for approving a proof if no corrections are required.

Inserts a selected stamp onto an appropriate place in the proof.

How to use it

- Click on the Add stamp icon in the Annotations section.
- Select the stamp you want to use. (The Approved stamp is usually available directly in the menu that appears).
- Click on the proof where you'd like the stamp to appear. (Where a proof is to be approved as it is, this would normally be on the first page).

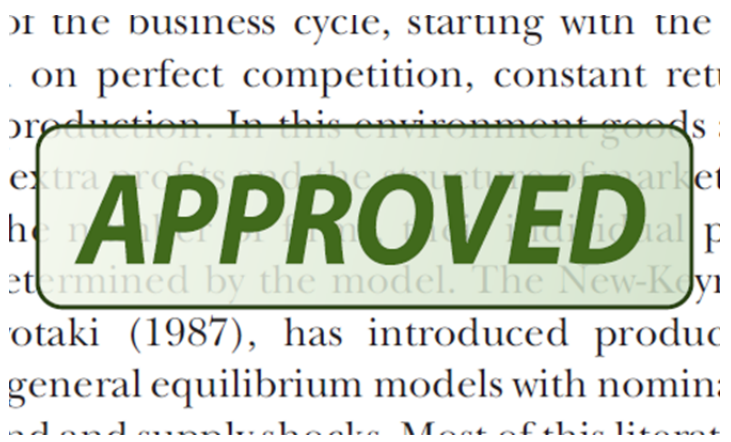

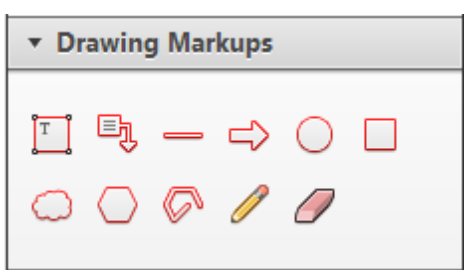

7. Drawing Markups Tools – for drawing shapes, lines and freeform annotations on proofs and commenting on these marks.

Allows shapes, lines and freeform annotations to be drawn on proofs and for comment to be made on these marks..

How to use it

- Click on one of the shapes in the Drawing Markups section.
- Click on the proof at the relevant point and draw the selected shape with the cursor.
- To add a comment to the drawn shape, move the cursor over the shape until an arrowhead appears.
- Double click on the shape and type any text in the red box that appears.

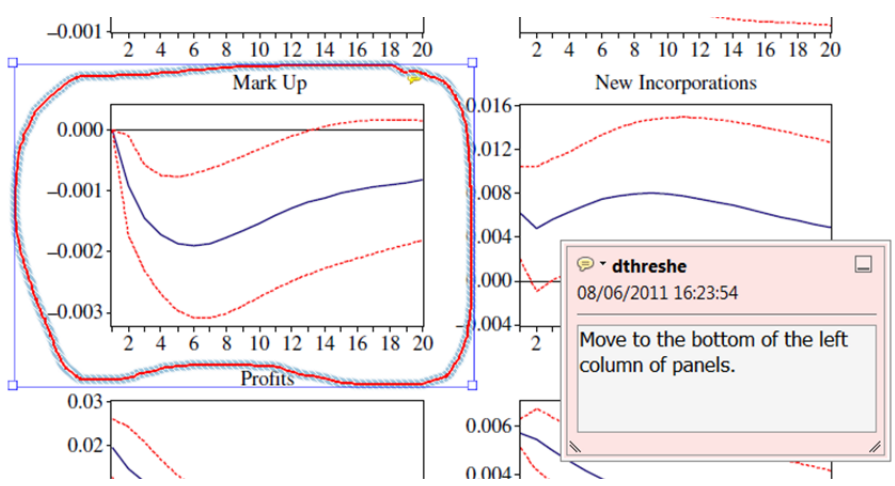

For further information on how to annotate proofs, click on the Help menu to reveal a list of further options: